

High-Capacity Angularly-Multiplexed Holographic Memory Operating at the Single Photon Level

Radosław Chrapkiewicz, Michał Dąbrowski,* and Wojciech Wasilewski
*Institute of Experimental Physics, Faculty of Physics,
University of Warsaw, Pasteura 5, 02-093 Warsaw, Poland*

(Dated: July 2, 2018)

We experimentally demonstrate an angularly-multiplexed holographic memory capable of intrinsic generation, storage and retrieval of multiple photons, based on off-resonant Raman interaction in warm rubidium-87 vapors. The memory capacity of up to 60 independent atomic spin-wave modes is evidenced by analyzing angular distributions of coincidences between Stokes and time-delayed anti-Stokes light, observed down to the level of single spin-wave excitation during several- μ s memory lifetime. We also propose how to practically enhance rates of single and multiple photons generation by combining our multimode emissive memory with existing fast optical switches.

PACS numbers: 42.50.Ex, 42.50.Ct, 32.80.Qk

Construction of on-demand sources of desired quantum states of light remains an overarching goal for quantum engineering. While single photons are essential resource for quantum communication protocols [1, 2], multiple photon states offer an avenue for quantum computing with linear optics [3, 4] and quantum simulations, e.g. in boson sampling schemes [5, 6]. Since scientists are already able to manufacture complex photonic chips using femtosecond writing technologies [7], perhaps the last major roadblock to perform linear-optics simulations unattainable by classical computing is the ability to create large number of photons capable of non-classical interference [8].

Prospective solutions to achieve this non-trivial, long-standing goal rely on still developing quantum dot sources [9–11], Rydberg blockade [12, 13] as well as parametric processes such as four-wave mixing [14] and spontaneous parametric down-conversion (SPDC) routinely employed to produce heralded single photons [15]. The present technology of SPDC sources is well developed and widespread since, while operating in room temperatures, it offers high brightness and renders low noise. Nonetheless, the intrinsic feature of parametric sources is their purely stochastic operation. The probability of photon pairs generation must be kept low to suppress the contribution of higher numbers of photons. A possible way to surpass this stochastic behavior is to combine multiple sources with fast, active optical switches [16, 17] to increase chances for single photon generation. In practice, setups with at most four sources using SPDC [18, 19] and twelve sources with cold atoms [20] have been demonstrated. Furthermore, N parametric sources can be used to generate N heralded photons but this method requires very long waiting time [18] as the probability for N -photon state generation falls exponentially with N .

Recently, Nunn *et al.* [21] have suggested a possible solution for enhanced generation of N -photon states in a system with N quantum memories storing heralded photons from N independent SPDC sources, and releasing

them at once. Here we present a different approach where photons can be generated directly inside many emissive quantum memories driven by Raman scattering process where deposition of an excitation is heralded by a detection of a Stokes photon. Moreover, as depicted in Fig. 1(a-c), multiple memories are implemented in our experiment within one atomic ensemble which serves as a single holographic memory interfacing many overlapping spin-wave modes of different spatial periodicity with independent angular modes of light. Presented angular multiplexing of many modes provides a tremendous simplification of experimental setups as compared with hypothetical multiple stand-alone memory systems.

Similarly as in SPDC sources the probability ζ of generating single excitation in any of memory modes has to be low, to suppress the probability ζ^2 for generating two excitations. However, if the number of available emissive modes M is large, the probability of photon generation in at least one of them $1 - (1 - \zeta)^M$ can approach unity [17]. For instance for $\zeta = 10^{-2}$, $M = 100$ the probability for Stokes photon generation reaches 60%. Once a photon is emitted in any of M modes, one can use an active optical switch [16, 17] seeded by triggering signal from the Stokes scattering, to route the anti-Stokes photon to a desired single output, as illustrated in Fig. 1(d). Such operation essentially relies on a memory storage time which has to exceed nanoseconds-long reconfiguration time of the optical switch [16, 17].

Note that probability for M modes to generate exactly N photons $\binom{M}{N} \zeta^N (1 - \zeta)^{M-N}$ can be also high. For $N = 8$, $M = 100$ it reaches a value of 7×10^{-6} which is over ten orders of magnitude larger than probability to obtain 8 photons from eight independent sources $\zeta^8 = 10^{-16}$. The scheme of Fig. 1(d) could be upgraded with a multiple-outputs switch. This way, after each successful generation of N excitations, the same multiphoton state of the product form $|1\rangle \otimes \dots \otimes |1\rangle$ can be produced in a desired set of output fibers. Most of the elements of this scheme such as matrices of single photon detectors,

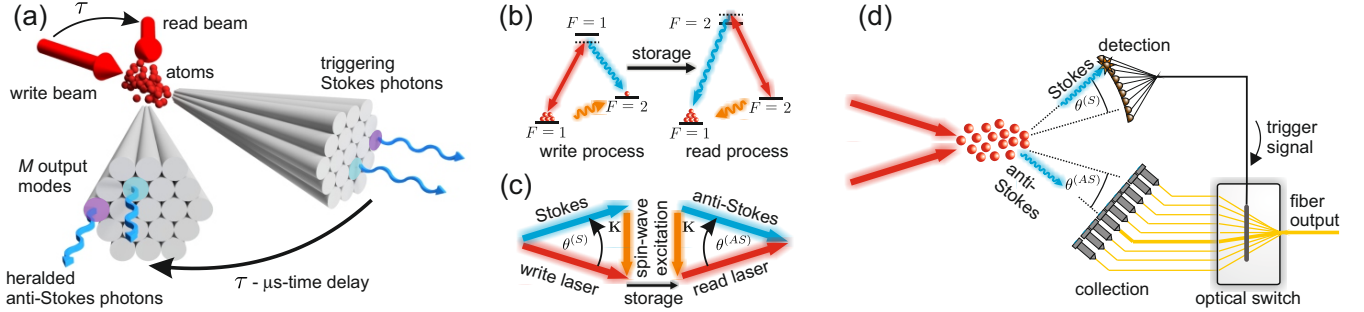


FIG. 1. (a) Idea of holographic memory generating, storing and releasing on-demand angularly correlated photons. Photons are produced in $2 \times M$ modes which are pairwise coupled. In each independent pair of modes (e.g. colored circles), anti-Stokes photons are heralded by Stokes photons generation, with μ s-time delay advance. (b) Generation and retrieval of photons is performed in Raman scattering process, using Λ -system ^{87}Rb energy levels. (c) Phase-matching condition relates wave-vectors of driving laser beams, photons and spin-wave excitation and determines the scattering angle of an anti-Stokes photon $\theta^{(\text{AS})} \simeq -\theta^{(\text{S})}$. (d) Predictability of scattering angles of anti-Stokes photons can be utilized to match outgoing photons to optical switch [16, 17] with one or multiple outputs (not shown). Switch architecture is reconfigured after detection of the Stokes trigger photons so as to pass single or N -photons into desired fiber links.

fiber bundles and fast optical switches have been demonstrated or are commercially available. The centerpiece is the multiplexed source of heralded photons with sufficient time-delay, based on spatial [20], temporal [22, 23] or another degree of freedom.

In this Letter we experimentally demonstrate a holographic atomic memory that can generate, store and retrieve light at the single photon level in many independent angular modes whose number could practically reach thousands [24] under realistic experimental conditions. Rather than using external non-deterministic sources of spectrally-filtered, heralded photons to convert them to atomic collective excitations [25], the Stokes photon generated inside the memory heralds the spin-wave creation which can be retrieved on demand in the time-delayed anti-Stokes scattering process. Combination of large number of emissive modes with predictability offered by a memory time-delay can circumvent the limits of SPDC sources and serve as an enhanced-rate source of photons. Moreover, our approach bridges the gap between numerous experiments with warm atomic memories with single spatial mode of light at the single photon level [25–28] and a few spatially multimode experiments performed at macroscopic light levels [29, 30].

Operation of our memory presented in Fig. 1(a-c) relies on collective multimode Raman scattering in atomic vapors in a DLCZ scheme [1]. The angular correlations between Stokes and anti-Stokes photons, mediated by phase-matching conditions depicted in Fig. 1(c), arise in a way similar to holography [31]. Firstly we write to the memory by driving spontaneous Raman transition in Λ -system, producing pairs of collective atomic excitation and spontaneous Stokes photon scattered in random direction. The write process resembles registering of a hologram and depending on the Stokes photon scattering

angle $\theta^{(\text{S})}$ the spin-wave with wave-vector $\mathbf{K} = 2\pi\theta^{(\text{S})}/\lambda$ is created, where λ stands for a wavelength of a driving beam. Then, after adjustable storage time τ , the atomic excitation can be converted to anti-Stokes photon with up to $\eta_{\text{read}} = 30\%$ internal read efficiency [27, 32, 33]. The read process is analogous to reconstruction of a hologram and the angle of the anti-Stokes photon emission $\theta^{(\text{AS})} \simeq -\theta^{(\text{S})}$ is determined by the preceding detection of the Stokes photon direction, a few microseconds in advance. Remarkably, the holographic storage allows us to populate, store and retrieve multiple overlapping yet independent spin-wave modes in the same ensemble of atoms.

The simplified scheme of the experimental setup is

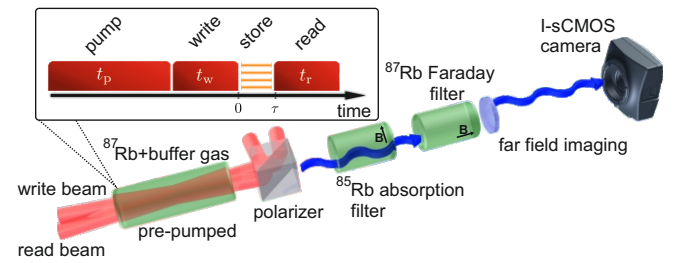


FIG. 2. The simplified scheme presenting key parts of the experimental setup for the holographic memory. Generation and storage of photons are implemented in warm ^{87}Rb vapors whose thermal motion is slowed down by admixture of noble buffer gas. Inset: experimental sequence. The triple filtering system [35] (polarization and two-step spectral, \mathbf{B} denotes magnetic field vector) passes scattered photons at different angles and blocks all laser beams detuned by 6.8 GHz. Detection of photons with high angular resolution is performed with an intensified sCMOS camera (I-sCMOS) capable of resolving photon coincidences [33, 36].

depicted in Fig. 2 (cf. [34, 35] for details). We pump atoms into $5^2S_{1/2}$, $F = 1$ and drive Raman transition to $5^2S_{1/2}$, $F = 2$ level. The driving lasers detuning was approximately 700 MHz from $5^2P_{1/2}$, $F = 1$ or $5^2P_{3/2}$, $F = 2$ levels as marked in Fig. 1(b). The main glass cell of $L = 10$ cm length was filled with ^{87}Rb mixed with krypton at 1 Torr and heated to $60^\circ - 75^\circ$ C corresponding to optical depths (OD) from 50 up to 80. The $1/e^2$ diameters of the linearly polarized driving beams at 795 nm or 780 nm tilted by 10 mrad inside the cell were about $2w = 4.6$ mm while the pump beam at 780 nm was twice as large. The typical experimental sequence depicted in the inset of Fig. 2 consists of pulses of 70 mW pump, 20 mW write and 15 mW read laser of duration: $t_p \approx 1$ ms, $t_w \simeq t_r \approx 1 \mu\text{s}$ while storage period is varied in the range $0 \leq \tau \leq 40 \mu\text{s}$. The triple filtering system — Wollaston prism, atomic absorption filter and Faraday filter (cf. [35] for details) is used to perform coincidence measurements at the single photon level. Essential advantage of our solution over routine spectral filtering using Fabry-Perot interferometers, is its transmission being insensitive to a photon scattering angle. We obtain large transmission of ca. 50% for both Stokes and anti-Stokes photons while attenuating 6.8 GHz detuned driving beams by the factor of 10^{11} . Moreover narrow spectral windows of the Faraday filter suppress the broadband collisional fluorescence [26] by at least two orders of magnitude and virtually blocks contribution from the four-wave mixing during read process [32]. Finally, we split Stokes from anti-Stokes using interference filters and angularly resolve them with suitable focusing lenses. Each field is directed to a separate regions on the intensified scientific CMOS (I-sCMOS) camera [33, 36, 37] used for counting coincidences.

Exemplary, raw single-shot images of the Stokes and the 500 ns-delayed anti-Stokes scattering are presented in Fig. 3(a). Visibly separated spots originate from multiple Raman scattered photons impinging the camera image intensifier where they are converted to bright phosphor flashes. The registered photons are noticeably grouped in speckle-like patterns [34] which in the anti-Stokes process are angularly-inverted as compared to the Stokes scattering, following the phase matching condition in Fig. 1(c). Here we exemplify an outcome of a high-gain Raman process where hundreds of photons are scattered in each shot, for $t_w = 2 \mu\text{s}$, $t_r = 1 \mu\text{s}$ and $\text{OD} = 80$. Thereafter we decreased the number of Stokes scattered photons whose mean number depends exponentially (high-gain) on write pulse duration t_w and OD. From each captured frame we extract the coordinates of individual photon detection events $\boldsymbol{\theta}^{(S)} = (\theta_x^{(S)}, \theta_y^{(S)})$, $\boldsymbol{\theta}^{(AS)} = (\theta_x^{(AS)}, \theta_y^{(AS)})$ for Stokes and anti-Stokes separate camera regions, with a real-time software processing [36, 37] as visualized in Fig. 3(b). An exemplary processed frame in the low-gain regime for $t_w = 250$ ns, $t_r = 500$ ns and $\text{OD} = 50$ is shown in Fig. 3(c).

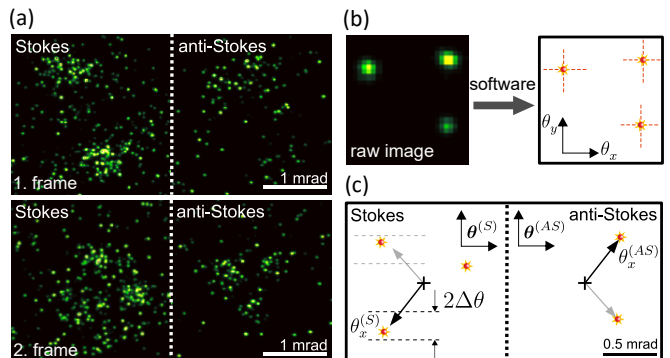


FIG. 3. (a) Two exemplary cropped frames with Stokes and 500 ns-delayed anti-Stokes photons detected as bright spots on I-sCMOS camera. Hundreds of angularly-resolved photons from a high-gain Raman scattering form pairwise inverted random patterns. (b) Real-time software algorithm converts with sub-pixel resolution raw I-sCMOS images into sets of coordinates representing central positions of individual single photon spots [36]. (c) Exemplary processed frame with several photons scattered in a low-gain regime. We further accumulate histograms of photon coordinates $n_{\text{coinc}}(\theta_x^{(S)}, \theta_x^{(AS)})$ for coincidences where detected anti-Stokes photon was preceded by a Stokes trigger found in a stripe fulfilling phase-matching condition $\theta_y^{(S)} = -\theta_y^{(AS)} \pm \Delta\theta$, where $\Delta\theta = 0.15$ mrad or 0.3 mrad. Black crosses mark driving beams directions.

We quantify the angular properties of the Raman scattering by measuring and analyzing distributions of coincidences $n_{\text{coinc}}(\boldsymbol{\theta}^{(S)}, \boldsymbol{\theta}^{(AS)})$ between the Stokes and time-delayed anti-Stokes photons. To confirm the angular correlations between time-delayed photons $\boldsymbol{\theta}^{(AS)} \simeq -\boldsymbol{\theta}^{(S)}$ it is convenient to display and focus on bidimensional coincidence distributions such as $n_{\text{coinc}}(\theta_x^{(S)}, \theta_x^{(AS)})$, equivalent to measurement with two one-dimensional detectors, cf. [38]. As illustrated in Fig. 3(c), to utilize all photons detected in two-dimensional camera frames we take into account photon pairs that appear in conjugate θ_y -separated stripes such as $|\theta_y^{(S)} + \theta_y^{(AS)}| < \Delta\theta$, integrating over $\theta_y^{(S)}, \theta_y^{(AS)}$ coordinates:

$$n_2(\theta_x^{(S)}, \theta_x^{(AS)}) = \int_{\theta_y^{(AS)} - \Delta\theta}^{\theta_y^{(AS)} + \Delta\theta} d\theta_y^{(AS)} \int d\theta_y^{(S)} n_2(\boldsymbol{\theta}^{(S)}, \boldsymbol{\theta}^{(AS)}). \quad (1)$$

The total number of coincidences counted this way $n_2(\theta_x^{(S)}, \theta_x^{(AS)})$ is a sum of two factors: a total number of Stokes–anti-Stokes pairs $n_{\text{coinc}}(\theta_x^{(S)}, \theta_x^{(AS)})$ and accidental coincidences from uncorrelated noise $n_{\text{acc}}(\theta_x^{(S)}, \theta_x^{(AS)})$ whose spatial distribution reads as follows:

$$n_{\text{acc}}(\theta_x^{(S)}, \theta_x^{(AS)}) = \frac{1}{\mathcal{N}} \int_{\theta_y^{(AS)} - \Delta\theta}^{\theta_y^{(AS)} + \Delta\theta} d\theta_y^{(AS)} \int d\theta_y^{(S)} n_1(\boldsymbol{\theta}^{(S)}) n_1(\boldsymbol{\theta}^{(AS)}), \quad (2)$$

where $n_1(\boldsymbol{\theta}^{(S)})$, $n_1(\boldsymbol{\theta}^{(AS)})$ are distributions of number of photons collected in both camera regions and \mathcal{N} is the total number of frames. Therefore the number of Stokes–anti-Stokes pairs can be calculated by subtracting the Eq. (2) from Eq. (1) [38]. At the center of the distribution the accidental coincidences constitute about 58% of the total number of pairs.

In Fig. 4(a) we present histograms representing angular distribution of coincidences between Stokes and anti-Stokes photons $n_{\text{coinc}}(\theta_x^{(S)}, \theta_x^{(AS)})$ for three different storage times $\tau = 0.5, 3.5, 5.5 \mu\text{s}$, each obtained from 3×10^5 frames for $t_w = 1 \mu\text{s}$, $t_r = 1 \mu\text{s}$ and $\text{OD} = 80$, for high Raman gain ($\eta_{\text{read}} = 30\%$). The maximum number of Stokes–anti-Stokes generated pairs per mode per single shot translates here to about 40 after correcting for the setup transmission and the detection efficiency. Characteristic elongated anti-diagonal shapes attest the conjugation of opposite angles of Stokes and time-delayed anti-Stokes scattering resulting from the phase matching condition $\theta_x^{(AS)} \simeq -\theta_x^{(S)}$. The diagonal $1/e^2$ width of $2w_{\text{corr}} = 1.2 \text{ mrad}$, almost independent of a storage time, represents the angular spread of the mode of anti-Stokes emission conditioned on preceding Stokes localization. The anti-diagonal width $2w_{\text{avg}}$ represents a span of angles $\theta_x^{(AS)}$ where the anti-Stokes light is detected. It decreases during the storage due to diffusion of atoms in the buffer gas [30, 39] which in turn washes out dense fringes in the stored spin-hologram coupling to higher angles of scattering [33].

The estimated number of modes M of our memory can be taken as the ratio of the solid angle span of anti-Stokes to a single mode spread $M \simeq 2(w_{\text{avg}}/w_{\text{corr}})^2$ [34], taking into account full two-dimensional mode structure illustrated in Fig. 1(a). We calculate the number of modes M on respective coincidence distributions and in Fig. 4(b) we present its dependence on the storage time acquired from additional measurement series, together with curve fitting [33]. M dropped from 58 for an instantaneous retrieval to 12 after $2 \mu\text{s}$ storage time. In the inset we can observe that for the longer storage times the number of retrieved modes drops to 2 within about $20 \mu\text{s}$. The maximum value displayed in Fig. 4(b) is close to the Fresnel number of the atomic ensemble $\mathcal{F} = w^2/\lambda L \approx 66$ as can be expected from the theory $M \simeq \mathcal{F}$ [40]. We therefore envisage that by increasing beams diameter about 4 times up to 18 mm, retrieval of even 1000 modes should be realistic.

Finally, in Fig. 4(c) we demonstrate the operation of the memory at the single excitation level, where maximum number of pairs generated per shot per mode is about 5×10^{-2} , for $t_w = 250 \text{ ns}$, $t_r = 500 \text{ ns}$ and $\text{OD} = 50$ providing a low Raman gain ($\eta_{\text{read}} = 13\%$). Here coincidences distribution $n_{\text{coinc}}(\theta_y^{(S)}, \theta_y^{(AS)})$ acquired from 10^6 frames reveals the similar structure and consequently number of retrieved modes M as in the higher

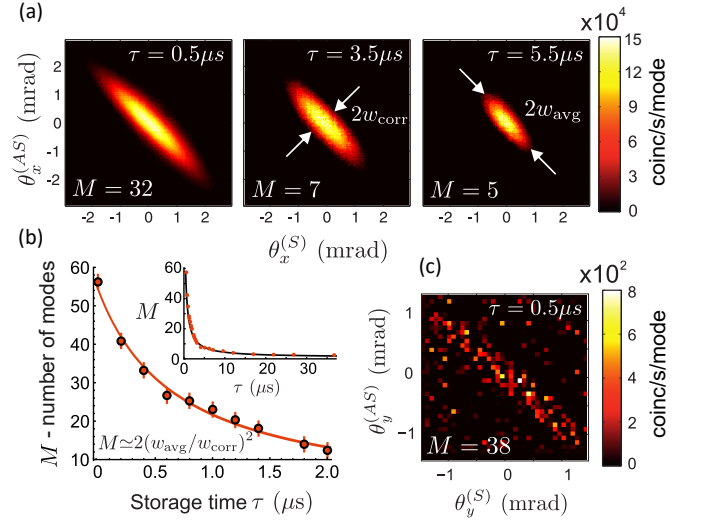


FIG. 4. (a) Angular distributions of Stokes and anti-Stokes photon coincidences $n_{\text{coinc}}(\theta_x^{(S)}, \theta_x^{(AS)})$ for increasing storage times τ reveal angular correlations $\theta_x^{(AS)} \simeq -\theta_x^{(S)}$ between photons stored and retrieved from the holographic memory. A visible decay of high-scattering-angle events is determined by a diffusional decoherence [39]. (b) A doubled squared ratio between anti-diagonal and diagonal width of coincidence histograms is used to estimate the total number of retrieved angular modes $M < 60 \simeq \mathcal{F}$ versus the storage time in agreement with diffusion model [33]. Tens of modes are retrieved within first $2 \mu\text{s}$, which is sufficiently long to couple the holographic memory source with currently existing optical switches [16, 17] (cf. Fig. 1(d)). Inset: a few modes can be retrieved up to tens of microseconds. (c) Coincidences are observable down to the single spin-wave excitation level.

gain regime. By keeping the probability for photon pair per mode low, here we generate on average ca. 0.9 Stokes–anti-Stokes pairs per shot in the whole memory [33]. This is an evidence of possible rate enhancement due to the mode multiplexing, while photons are $0.5 \mu\text{s}$ -delayed in time.

In both high and low-gain regimes we obtain the ratio of coincidences to overall registered pairs of approx. 42% which is comparable with single-spatial-mode warm atomic memories [25, 27, 28]. The noise of the same frequency as anti-Stokes photons originates primarily from collisions with buffer gas [41] that lead to isotropic and incoherent Stokes scattering in the read stage. Although an employment of even more stringent spectral filtering would further decrease a broadband noise component as shown in a single-spatial-mode system [28], we suspect that further demonstrations beyond proof of principle, aiming in practical N -photon source, may benefit from implementations in cold atomic systems where high non-classical correlations can be readily achieved [42–44].

In conclusion, we presented the first experimental demonstration of large number of angular modes from the emissive atomic memory that predictably generate anti-

Stokes photons in a direction known several microseconds in advance through the preceding detection of Stokes photons. In our implementation in warm rubidium-87 vapors we were generating, storing and retrieving light at the single photon level from up to 60 spin-wave modes whose number can be further scaled up with an increasing Fresnel number [24, 40]. From supporting measurements we infer that no more than one spin-wave per mode is present in the memory [33], but non-classical operation of the memory is not directly shown. We suggest that a combination of such multimode memory with existing optical switches [16, 17] will be a realistic method for enhanced-rate generation of single [45, 46] or N -photon states, the latter being a prerequisite for linear-optics quantum computing [3, 4] and simulations [5, 6]. Our work constitutes the first observation of time-delayed multimode angular correlations at the single photon level in contrast to all previous studies where such correlations were observed exclusively in instantaneous nonlinear processes [47], such as parametric down-conversion [48] or four-wave mixing [49].

Acknowledgments. We acknowledge discussions with A. Bogucki, M. Jachura, A. Leszczyński, M. Lipka, M. Mazelanik, M. Parniak and P. Ziń as well as support of K. Banaszek and J. Iwaszkiewicz. This project was financed by the National Science Center (Poland) (Grants No. DEC-2011/03/D/ST2/01941 and DEC-2015/19/N/ST2/01671), PhoQuS@UW (Grant Agreement No. 316244) and it was supported in part by PL-Grid Infrastructure. R.C. was supported by the Foundation for Polish Science.

* mdabrowski@fuw.edu.pl

- [1] L. M. Duan, M. D. Lukin, J. I. Cirac, and P. Zoller, *Nature* **414**, 413 (2001).
- [2] Z.-S. Yuan, Y.-A. Chen, B. Zhao, S. Chen, J. Schmiedmayer, and J.-W. Pan, *Nature* **454**, 1098 (2008).
- [3] E. Knill, R. Laflamme, and G. J. Milburn, *Nature* **409**, 46 (2001).
- [4] P. Kok, W. J. Munro, K. Nemoto, T. C. Ralph, J. P. Dowling, and G. J. Milburn, *Rev. Mod. Phys.* **79**, 135 (2007).
- [5] A. Peruzzo *et al.*, *Science* **329**, 1500 (2010).
- [6] K. R. Motes, A. Gilchrist, J. P. Dowling, and P. P. Rohde, *Phys. Rev. Lett.* **113**, 120501 (2014).
- [7] S. Gross and M. J. Withford, *Nanophotonics* **4**, 332 (2015).
- [8] M. Jachura, M. Karpiński, C. Radzewicz, and K. Banaszek, *Opt. Express* **22**, 8624 (2014).
- [9] O. Gazzano *et al.*, *Nat. Commun.* **4**, 1425 (2013).
- [10] X. Ding, *et al.*, *Phys. Rev. Lett.* **116**, 020401 (2016).
- [11] A. J. Bennett, *et al.*, *Sci. Adv.* **2**, e1501256 (2016).
- [12] T. Peyronel, *et al.*, *Nature* **488**, 57 (2012).
- [13] F. Ripka, Y.-H. Chen, R. Löw, and T. Pfau, *Phys. Rev. A* **93**, 053429 (2016).
- [14] O. Alibart, *et al.*, *New J. Phys.* **8**, 67 (2006).
- [15] A. B. U'Ren, C. Silberhorn, K. Banaszek, and I. A. Walmsley, *Phys. Rev. Lett.* **93**, 093601 (2004).
- [16] M. A. Hall, J. B. Altepeter, and P. Kumar, *Phys. Rev. Lett.* **106**, 053901 (2011).
- [17] X.-S. Ma, S. Zotter, J. Kofler, T. Jennewein, and A. Zeilinger, *Phys. Rev. A* **83**, 043814 (2011).
- [18] X.-C. Yao *et al.*, *Nat. Photon.* **6**, 225 (2012).
- [19] M. J. Collins *et al.*, *Nat. Commun.* **4**, 2582 (2013).
- [20] S.-Y. Lan, A. G. Radnaev, O. A. Collins, D. N. Matsukevich, T. A. Kennedy, and A. Kuzmich, *Opt. Express* **17**, 13639 (2009).
- [21] J. Nunn, *et al.*, *Phys. Rev. Lett.* **110**, 133601 (2013).
- [22] C. Simon, H. de Riedmatten, and M. Afzelius, *Phys. Rev. A* **82**, 010304 (2010).
- [23] B. Albrecht, P. Farrera, G. Heinze, M. Cristiani, and H. de Riedmatten, *Phys. Rev. Lett.* **115**, 160501 (2015).
- [24] A. Grodecka-Grad, E. Zeuthen, and A. S. Sørensen, *Phys. Rev. Lett.* **109**, 133601 (2012).
- [25] P. S. Michelberger *et al.*, *New J. Phys.* **17**, 043006 (2015).
- [26] C. H. van der Wal *et al.*, *Science* **301**, 196 (2003).
- [27] K. F. Reim, *et al.*, *Phys. Rev. Lett.* **107**, 053603 (2011).
- [28] M. Bashkansky, F. K. Fatemi, and I. Vurgaftman, *Opt. Lett.* **37**, 142 (2012).
- [29] D. B. Higginbottom, B. M. Sparkes, M. Rancic, O. Pinel, M. Hosseini, P. K. Lam, and B. C. Buchler, *Phys. Rev. A* **86**, 023801 (2012).
- [30] O. Firstenberg, M. Shuker, A. Ron, and N. Davidson, *Rev. Mod. Phys.* **85**, 941 (2013).
- [31] H.-N. Dai, *et al.*, *Phys. Rev. Lett.* **108**, 210501 (2012).
- [32] M. Dąbrowski, R. Chrapkiewicz, and W. Wasilewski, *Opt. Express* **22**, 26076 (2014).
- [33] See Supplemental Material at [URL] for the discussion of multimode retrieval properties and heralding efficiency of presented holographic memory.
- [34] R. Chrapkiewicz and W. Wasilewski, *Opt. Express* **20**, 29540 (2012).
- [35] M. Dąbrowski, R. Chrapkiewicz, and W. Wasilewski, *J. Mod. Opt.* **63**, 2029-2038 (2016).
- [36] M. Jachura and R. Chrapkiewicz, *Opt. Lett.* **40**, 1540 (2015).
- [37] R. Chrapkiewicz, W. Wasilewski, and K. Banaszek, *Opt. Lett.* **39**, 5090 (2014).
- [38] W. H. Peeters, J. J. Renema, and M. P. van Exter, *Phys. Rev. A* **79**, 043817 (2009).
- [39] R. Chrapkiewicz, W. Wasilewski, and C. Radzewicz, *Opt. Commun.* **317**, 1 (2014).
- [40] M. G. Raymer and J. Mostowski, *Phys. Rev. A* **24**, 1980 (1981).
- [41] S. Manz, T. Fernholz, J. Schmiedmayer, and J.-W. Pan, *Phys. Rev. A* **75**, 040101 (2007).
- [42] T. Chanelière, D. N. Matsukevich, S. D. Jenkins, S.-Y. Lan, T. A. B. Kennedy, and A. Kuzmich, *Nature* **438**, 833 (2005).
- [43] X.-H. Bao *et al.*, *Nat. Phys.* **8**, 517 (2012).
- [44] P. Farrera *et al.*, *Nat. Commun.* **7**, 13556 (2016).
- [45] D. N. Matsukevich, T. Chanelière, S. D. Jenkins, S.-Y. Lan, T. A. B. Kennedy, and A. Kuzmich, *Phys. Rev. Lett.* **97**, 013601 (2006).
- [46] C.-W. Chou, *et al.*, *Science* **316**, 1316 (2007).
- [47] D. E. Chang, V. Vuletić, and M. D. Lukin, *Nat. Photon.* **8**, 685 (2014).
- [48] O. Jedrkiewicz, *et al.*, *Phys. Rev. Lett.* **93**, 243601 (2004).
- [49] V. Boyer, A. M. Marino, R. C. Pooser, and P. D. Lett, *Science* **321**, 544 (2008).

SUPPLEMENTAL MATERIAL

I. HERALDING AND DETECTION EFFICIENCY

The efficiency of our quantum memory setup is limited by finite retrieval efficiency of the anti-Stokes light $\eta_{\text{read}}^{(\text{high})} = 0.3$ for stimulated (high-gain) regime or $\eta_{\text{read}}^{(\text{low})} = 0.13$ for spontaneous (low-gain) regime. The characteristic decay of signal scattered during the read process (see Fig. 5) depends on the write pulse duration and optical depth (OD). The effective retrieval time is limited by the diffusion, thus in the spontaneous regime we obtain lower read efficiency than for stimulated regime. We filtered out the four-wave mixing noise [S1] using Faraday filter with transmission $\eta_T = 0.5$ [S2], at the same time achieving the total heralding efficiency of $\eta_H^{(\text{high})} = 0.15$ or $\eta_H^{(\text{low})} = 0.07$.

This is comparable to other single-photon sources implemented using quantum memories. Single-photon-level quantum memory using room-temperature atomic vapors [S3] as well as cold atoms [S4] both achieve $\eta_H = 0.2$. In experiments with bulk diamond in room-temperature [S5] and hydrogen molecules [S6] picosecond storage times with heralding efficiency of $\eta_H = 0.16$ and $\eta_H = 0.18$ have been reported. Solid state spin-wave quantum memory for time-bin qubits with $\eta_H = 0.06$ has been recently constructed [S7]. Saunders *et al.* [S8] used external cavity to improve the ratio of signal of Raman scattered photons to noise from the four-wave mixing process and obtained $\eta_H = 0.1$.

Finite heralding efficiency η_H limits the chance of retrieving exactly N photons (by a factor of η_H^N) to $\eta_H^N \binom{M}{N} \zeta^N (1 - \zeta)^{M-N}$ where ζ is the probability of generating single excitation in any of M memory modes. With current heralding efficiency this would severely limit the N -photon production rate. However even this limited rate would be orders of magnitude faster for $N = 8$, $M = 100$ than the rate at which 8 SPDC sources fire simultaneously ζ^N , even assuming they approach perfect heralding limit $\eta_H \simeq 1$, if the pair production rate ζ is small enough to inhibit creation of double pairs from any source. Similarly as in SPDC sources, the source we propose can work only with post-selection.

The detection system we use is a commercially available sCMOS Andor Zyla 5.5 Mpx camera connected with Hamamatsu Image Intensifier (V7090D). The quantum efficiency of the whole system is QE=20%, a dark count rate of 2 counts per 1 μs image intensifier gate time for the whole camera region and with the shortest possible gating time of 100 ns.

II. TEMPORAL AND STATISTICAL PROPERTIES OF SCATTERED PHOTONS

In the main body of the article (see Fig. 4) we presented the coincidences between the photons scattered in the write and read processes at any angle. Due to the limitations of our detection system, the measurements of coincidences presented in the main manuscript were time integrated thus carrying no information about the arrival time of a photon [S9]. However, additional information about the timing of the photons can be gathered by gating the image intensifier for shorter periods of time. By scanning a short gate window of $\tau = 100$ ns duration across the write and read pulses we measured the temporal evolution of the average intensity of light scattered in write and read processes as depicted in Fig. 5.

The light scattered during write and read processes is separated with interference filters, cropped and focused on separate regions on the camera. We verified that the write region is not illuminated during read pulse and read region is not illuminated during write pulse. The measurement in Fig. 5 was done with write and read pulses longer than required for a single photon level. Note almost constant write intensity and an exponential decay $\exp(-\gamma_0 t)$ with $\gamma_0 = 3.82$ MHz of the average read intensity.

To scatter light at the single photon level (results presented in Fig. 4(c) of the main manuscript) the pulse durations were shortened to $t_w = 250$ ns and $t_r = 500$ ns for write and read pulses, as marked by dark shaded regions in Fig. 5. Virtually time independent intensity of scattered light in the write process is the signature of the spontaneous Stokes scattering regime. After about 500 ns the stimulated regime begins, where more than one photon is scattered per mode and the number of scattered photons start to grow exponentially with drive pulse en-

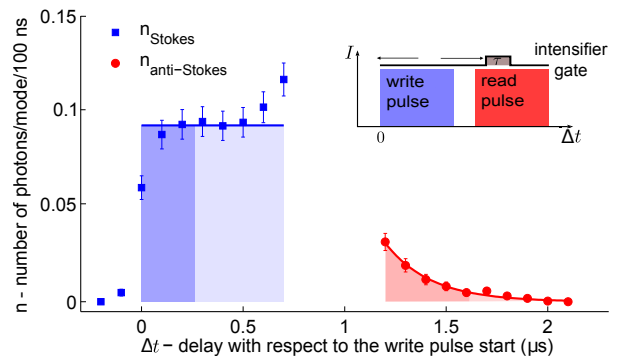


FIG. 5. Time evolution of photon number scattered per mode during 100 ns for $t_w = 700$ ns, $t_{\text{store}} = 500$ ns, $t_r = 800$ ns. Stokes photons are scattered in the spontaneous regime while anti-Stokes signal decay exponentially in time. The dark shadow regions correspond to the pulse sequence for results in Fig. 4(c) of the main manuscript. Inset: laser pulses and image intensifier pulse sequence.

ergy, due to the bosonic gain. Here a mode is defined as a portion of a light field and a corresponding spin-wave that are coupled exclusively to each other by a Raman interaction, thus their joint evolution can be described by two mode squeezing [S10], with squeezing parameter proportional to the drive field amplitude and the Raman coupling strength. For the size of the driving beams used in the experiment ($\pi w^2/\lambda \gg L$), the modes can be approximated by plane waves. The number of modes M can be estimated assuming atomic ensemble is a rectangular box with dimensions $w \times w \times L$.

Consider M -pairs of spin-wave and photon modes. The driving beam during Stokes scattering produces photon-spin-wave pairs with probability ζ in each mode. As long as $\zeta \ll 1$, the number of photons is a linear function of drive pulse energy and the total number of photons $\langle n \rangle = M\zeta$. Therefore, we are in the linear regime as long as the total number of photons is smaller than the number of modes: $\zeta M \ll M$. As compared with Fig. 5, we can see that indeed the photon production rate bends up when the average number of photons per angular mode becomes equal to 0.47.

Figure 4(c) depicted the situation with 0.9 Stokes–anti-Stokes photon pairs in the whole memory volume. Taking into account the read efficiency in the low-gain regime $\eta_{\text{read}}^{(\text{low})} = 0.13$, we generated 6.9 Stokes–spin-wave pairs during the write stage which for $M = 38$ angular modes corresponds to the 0.18 generated photon–spin-wave pairs per mode. That situation can be compared with the results depicted in Fig. 5 where the dark shadow regions represent the situation from Fig. 4(c). After 250 ns (which is still in the spontaneous regime) the total number of scattered photons is 0.21 per angular mode. The number of modes produced in the write process is about $M = 130$. The results are corrected for finite heralding, detection and read efficiency and the fact that only c.a. 40% of the scattered light produce spin-wave excitations [S2].

This reinforces our statement that for a pulse duration of 250 ns, on average no more than a single photon–spin-wave pair is created per mode. In turn exponential decay of the read light confirms conversion of the stored spin-waves to light [S1]. Because in the low-gain regime 58% of the total number of detected pairs are accidentals, it is extremely hard to detect non-classical cross-correlations [S11] between the photons.

We also conducted correlation measurements for pulse sequence depicted in Fig. 5 and gate pulses either: containing whole write, or second half of write, first half or whole read pulse. The strongest correlations are found between Stokes and anti-Stokes light scattered during whole write and read pulses. The Stokes–anti-Stokes correlations during whole write and first half of the read pulse are almost of the same strength. The correlations during second half of the write pulse and the either whole or first half of the read are notably weaker though. This

is in concert with the observation that the write operation lasts for the entire pulse, while the read is decaying fast.

In summary, all the above evidence supports the conclusion that the information is being transferred from the Stokes scattering to the anti-Stokes scattering occurring afterwards.

III. DECAY OF THE MODE NUMBER IS DUE TO DIFFUSION

We quantify the angular properties of the Raman scattering by measuring and analyzing distributions of coincidences $n_{\text{coinc}}(\boldsymbol{\theta}^{(\text{S})}, \boldsymbol{\theta}^{(\text{AS})})$ between the Stokes and time-delayed anti-Stokes photons, where for simplicity we focus on bidimensional coincidence distributions such as $n_{\text{coinc}}(\theta_x^{(\text{S})}, \theta_x^{(\text{AS})})$. The correlation maps presented in Fig. 4(a) of the main manuscript are virtually 2D gaussians with standard deviations $\sigma_1(t)$ and $\sigma_2(t)$ of the form:

$$n_{\text{coinc}}(t) = n_0 \exp\left(-\frac{(\theta_x^{(\text{S})} + \theta_x^{(\text{AS})})^2}{2\sigma_1^2(t)} - \frac{(\theta_x^{(\text{S})} - \theta_x^{(\text{AS})})^2}{2\sigma_2^2(t)}\right). \quad (3)$$

The diffusion attenuates the spin-waves with wave-vector \mathbf{K} at a rate $\gamma(\mathbf{K}) = D|\mathbf{K}|^2$ where D is the diffusion coefficient. Due to attenuation of spin-waves, the read photons are scattered in narrower range of angles $\theta_x^{(\text{AS})}$. Therefore the number of coincidences decays with time:

$$n_{\text{coinc}}(t) = n_{\text{coinc}}(0) \exp\left(-2Dt \left(\frac{2\pi}{\lambda} \theta_x^{(\text{AS})}\right)^2\right). \quad (4)$$

Thus both variances σ_1^2 and σ_2^2 decay according to $[\sigma_i^2(t)]^{-1} = [\sigma_i^2(0)]^{-1} + 8\pi^2 Dt/\lambda^2$, $i = 1, 2$.

We also take into consideration the finite angular extent (finite spatial size) of the read laser beam diameter

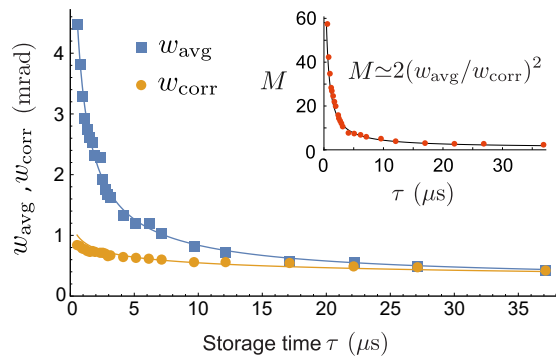


FIG. 6. Variances of coincidence distribution in diagonal w_{avg} and anti-diagonal w_{corr} directions versus storage time τ . Inset: estimated number of modes stored inside the memory. Compare Fig 4(b) of the main manuscript.

$2w$ which means the angular distribution we finally register $\tilde{n}_{\text{coinc}}(\theta_x^{(S)}, \theta_x^{(AS)}, t)$ is described by the convolution of the atomic contribution $n_{\text{coinc}}(\theta_x^{(S)}, \theta_x^{(AS)}, t)$ and the gaussian angular spread of the read laser pulse:

$$\tilde{n}_{\text{coinc}}(t) = n_{\text{coinc}}(t) * \exp\left(\frac{-(\theta_x^{(AS)})^2}{w^2}\right). \quad (5)$$

From the above formula we calculate the widths w_{avg} and w_{corr} in diagonal and anti-diagonal directions, respectively.

The estimated number of modes M retrieved from our memory can be taken as the ratio of the solid angle span of anti-Stokes to a single mode spread $M \simeq 2(w_{\text{avg}}/w_{\text{corr}})^2$ [S12], taking into account full two-dimensional mode structure. Such a figure of merit is completely equivalent with the entanglement dimension coefficient \mathbf{D} [S13], with the correspondence $M = 2\mathbf{D}$.

The Fig. 6 (see Fig. 4(b) of the main manuscript) presents the decay of both widths w_{avg} and w_{corr} with time together with theoretical curve obtained from the above formulas. The decay of the number of modes M with time is due to diffusion, but it is not exponential.

IV. INDEPENDENCE OF MODES

Different modes of atomic spin-wave excitations remain independent during storage time and any cross-influence of modes can be excluded. This is evidenced by the same angular spread of anti-Stokes light, conditioned on certain Stokes direction - regardless on the storage time (see Fig. 4(a) of the main manuscript).

The diffusion picture reinforces this statement. A flat plane spin-wave with wave-vector \mathbf{K} will decay due to diffusion, but its wave-vector will not be changed and will not spread. In our experiment we create spin-waves of 3.2 mm diameter by detecting scattered light in the far field. Upon creation they consist of a range of wave-vectors around central \mathbf{K} . Due to diffusion the initial distribution in the momentum space will be distorted towards small \mathbf{K} , however will never get broader than it was initially. Therefore two neighboring (in \mathbf{K} space) modes will never cross talk. Alternatively, we can consider the cell in the position representation: both neighboring modes diffuse in time - their coherence spreads over more and more volume. Nonetheless the spin-wavefronts directions remain the same, implying that the overlap of the modes never rises.

It is worthwhile to consider how the atoms carry the information contained in the spin-waves. In our scheme

any atom is potentially carrying information about each illuminated mode. This situation can be opposed to [S14] where the atomic cloud was divided into 12 memories one next to the other. In that experiment, where spatial, not angular modes were used, the total number of atoms was practically split to form twelve separate ensembles. It is noteworthy that with the configuration from [S14], after very long storage times the atoms from one spatial region may diffuse to neighboring spatial regions.

With the same thermal speed of atoms or diffusion coefficient D both methods (our and that presented in [S14]) give the same OD for the same number of modes for the same storage time. In our method the ensemble diameter is divided by the number of modes to get the maximal distance the atoms can travel before the highest mode is washed out. If multiple separate ensembles are used, the diameter of each has to be smaller than this distance. Thus the atoms have to fill the same cross section area, leading to the same OD.

* mdabrowski@fuw.edu.pl

- [S1] M. Dąbrowski, R. Chrapkiewicz, and W. Wasilewski, *Opt. Express* **22**, 26076 (2014).
- [S2] M. Dąbrowski, R. Chrapkiewicz, and W. Wasilewski, *J. Mod. Opt.* **63**, 2029-2038 (2016).
- [S3] K. F. Reim, P. Michelberger, K. C. Lee, J. Nunn, N. K. Langford, and I. A. Walmsley, *Phys. Rev. Lett.* **107**, 053603 (2011).
- [S4] P. Farrera *et al.*, *Nat. Commun.* **7**, 13556 (2016).
- [S5] D. G. England *et al.*, *Phys. Rev. Lett.* **114**, 053602 (2015).
- [S6] P. J. Bustard, R. Lausten, D. G. England, and B. J. Sussman, *Phys. Rev. Lett.* **111**, 083901 (2013).
- [S7] M. Gündoğan, P. M. Ledingham, K. Kutluer, M. Mazzera, and H. de Riedmatten, *Phys. Rev. Lett.* **114**, 230501 (2015).
- [S8] D. Saunders *et al.*, *Phys. Rev. Lett.* **116**, 090501 (2016).
- [S9] M. D. Eisaman, A. André, F. Massou, M. Fleischhauer, A. S. Zibrov, and M. D. Lukin, *Nature* **438**, 837 (2005).
- [S10] J. Kołodźński, J. Chwedeńczuk, and W. Wasilewski, *Phys. Rev. A* **86**, 013818 (2012).
- [S11] B. Albrecht, P. Farrera, G. Heinze, M. Cristiani, and H. de Riedmatten, *Phys. Rev. Lett.* **115**, 160501 (2015).
- [S12] R. Chrapkiewicz and W. Wasilewski, *Opt. Express* **20**, 29540 (2012).
- [S13] M. P. Edgar *et al.*, *Nat. Commun.* **3**, 984 (2012).
- [S14] S.-Y. Lan, A. G. Radnaev, O. A. Collins, D. N. Matsukevich, T. A. Kennedy, and A. Kuzmich, *Opt. Express* **17**, 13639 (2009).